The immune microenvironment and neoantigen landscape of aggressive salivary gland carcinomas differ by subtype

Maximilian Linxweiler[1], Fengshen Kuo[2], Nora Katabi[3], Mark Lee[1], Zaineb Nadeem[1], Martin G. Dalin[1,4], Vladimir Makarov[1,2], Diego Chowell[1,2], Snjezana Dogan[3], Ian Ganly[5], A. Ari Hakimi[5], Richard J. Wong[5], Nadeem Riaz[2,6], Alan L. Ho[7], Timothy A. Chan[1,2,6+], Luc G.T. Morris[1,2,5+]

[+]Corresponding authors

1. Human Oncology and Pathology Program, Memorial Sloan Kettering Cancer Center, New York, NY
2. Immunogenomics and Precision Oncology Platform, Memorial Sloan Kettering Cancer Center, New York, NY
3. Department of Pathology, Memorial Sloan Kettering Cancer Center, New York, NY
4. Department of Pediatrics, Institute of Clinical Sciences, University of Gothenburg, Gothenburg, Sweden
5. Department of Surgery, Memorial Sloan Kettering Cancer Center, New York, NY
6. Department of Radiation Oncology, Memorial Sloan Kettering Cancer Center, New York, NY
7. Department of Medicine, Memorial Sloan Kettering Cancer Center, New York, NY

Conflicts of interest: TAC is a co-founder of and holds equity in Gritstone Oncology and received research funding from Bristol Myers Squibb, Eisai, AstraZeneca and Illumina. ALH received funding from Eisai, BMS, Kura Oncology, AstraZeneca, Genentech Roche, Celldex, Pfizer, Lilly, Bayer, consulting fees from BMS, Merck, Novartis, AstraZeneca, Regeneron, Sanofi Aventis, Sun Pharmaceuticals, Eisai, Genentech/Roche, Genzyme, Ayala Pharmaceuticals, and travel reimbursement from Ignyta, Kura Oncology. LGTM received laboratory research funding from Illumina, Inc. and AstraZeneca.

Running title: immune microenvironment of salivary gland cancer

Corresponding authors:
Timothy A. Chan or Luc G.T. Morris
Immunogenomics and Precision Oncology Platform
Memorial Sloan Kettering Cancer Center
New York, NY, 10065
Phone: 212-639-3049 Fax: 646-888-2595

Email: morrisl@mskcc.org or chant@mskcc.org

Translational Relevance: In this study, we characterize the immune microenvironment and neoantigen landscape of salivary gland cancers using RNA sequencing in 76 tumors representing the 3 most lethal histologies: adenoid cystic carcinoma (ACC), myoepithelial carcinoma (MECA), and salivary duct carcinoma (SDC). We show that SDCs exhibited high levels of immune infiltration, with corresponding higher levels of T cell dysfunction, and higher mutational load. ACCs were characterized by an immune-excluded microenvironment, the presence of M2-polarized macrophages and myeloid-derived suppressor cells, and very low mutational load. MECAs were more heterogeneous, with both immune-low and immune-high phenotypes. Across all SGCs, immune infiltration was associated with mutation- and fusion-derived neoantigens. These findings provide new insights into the immune microenvironment and neoantigen landscape of SGCs, showing that mechanisms of immune escape differ by histology. These data nominate potential immunologic vulnerabilities and may help guide the next steps of investigation in precision immunotherapy for these difficult-to-treat cancers.

Abstract

Purpose: Salivary gland carcinomas (SGCs) are rare, aggressive cancers with high rates of recurrence and distant metastasis. These factors, and a lack of active systemic therapies, contribute to poor clinical outcome. Response rates with immune checkpoint blockade have been low, although clinical data remain sparse. To improve the efficacy of therapies, a more comprehensive understanding of relevant molecular alterations and immunologic processes is needed.

Experimental Design: To characterize the immune microenvironment and neoantigen landscape of SGCs, we performed RNA sequencing (RNAseq) in 76 tumors representing the 3 most lethal histologies: adenoid cystic carcinoma (ACC), myoepithelial carcinoma (MECA), and salivary duct carcinoma (SDC). We analyzed transcriptomic profiles, tumor-infiltrating immune cell populations, and measures of T cell activation/dysfunction. In 37 cases also undergoing exome sequencing, we analyzed somatic mutations and neoantigens.

Results: SDCs exhibited high levels of immune infiltration, with corresponding higher levels of T cell dysfunction, and higher mutational load. In contrast, ACCs were characterized by an immune-excluded microenvironment, the presence of M2-polarized macrophages and myeloid-derived suppressor cells, and very low mutational load. MECAs were more heterogeneous, with both immune-low and immune-high phenotypes represented. Across all SGCs, levels of immune infiltration were associated with mutation- and fusion-derived neoantigens, and with aggressive clinical behavior.

Conclusions: These findings provide new insights into the immune microenvironment and neoantigen landscape of SGCs, showing that mechanisms of immune escape appear to differ by histology. These data nominate potential immunologic vulnerabilities and may help guide the next steps of investigation in precision immunotherapy for these difficult-to-treat cancers.

Key words: salivary gland cancer, immune microenvironment, neoantigens, transcriptional pathways, immunotherapy

Introduction

Salivary gland carcinomas (SGCs) arise from the major salivary glands (parotid, submandibular, sublingual), or the minor salivary glands of the upper aerodigestive tract. They are a heterogeneous group of malignancies, with 20 subtypes defined by the World Health Organization[1]. The standard therapy for salivary gland cancers is surgical resection, with adjuvant radiotherapy or chemoradiotherapy in some cases – an approach that successfully treats a subset of patients. However, disease recurrence or metastasis is common, with distant metastases occurring in 25–50% of patients[2]. Because there are no active systemic therapies for SGCs, recurrent or metastatic disease is usually incurable. Ultimately the 5-year survival rate of recurrent/metastatic SGC is only approximately 20%.

Due to their relative rarity (incidence approximately 1 per 100,000 persons), the molecular features of these tumors are only beginning to be characterized, and features of their immune microenvironment have not been well defined. To improve the effectiveness of treatment, including immunotherapy, a better understanding of how SGCs evade immune surveillance is needed.

In terms of risk of relapse, the 3 most aggressive histological subtypes of salivary gland tumors are adenoid cystic carcinoma (ACC), myoepithelial carcinoma (MECA), and salivary duct carcinoma (SDC). Each of these cancers exhibits a high rate of recurrence, distant metastasis, and resistance to conventional therapy.

ACCs account for approximately 10% of salivary gland malignancies[3], have low numbers of mutations, but have oncogenic fusions of *MYB-NFIB* or *MYBL1-NFIB* in approximately 60% of cases[4-6]. There are no highly active systemic therapies for ACC.

MECAs are rare (~2%) salivary gland tumors with a highly heterogeneous composition of cells[7]. Like ACCs, MECAs are also characterized by low mutational burden and a high prevalence of oncogenic gene fusions, many of which include *PLAG1* [8]. There are no effective systemic therapies for MECA.

SDCs account for 1–3% of all salivary gland tumors[9]. Morphologically, these tumors resemble invasive ductal carcinoma of the breast, with a molecular profile similar to apocrine breast cancer [10]. They often overexpress androgen receptor (AR) or ERBB2

(HER2)[11], both of which appear in early data to be targetable[12], although clinical trials are ongoing. Targetable mutations in the PIK3CA and MAPK pathways have also been identified[10,13].

In recent years, drugs that inhibit T cell checkpoints such as CTLA-4 and the PD-1/PD-L1 axis have shown activity and achieved clinically meaningful responses in a subset of patients with different tumor types including melanoma, non-small cell lung, kidney, bladder and urothelial carcinomas, as well as microsatellite instability-high carcinomas of various sites [14-21]. In head and neck squamous cell carcinoma, anti-PD-1 therapies have achieved clinical responses in 15–20% of patients[22-24].

To date, there is only sparse data regarding the activity of immune checkpoint blockade in SGCs. The KEYNOTE-028 basket trial of PD-L1 positive tumors included a small salivary gland cancer cohort of 28 patients treated with pembrolizumab. Despite enrichment for PD-L1 positive tumors, there was a modest overall response rate of 12% (all in non-ACC adenocarcinoma histologies), with a 6-month progression-free survival of 21%[25].

Recently, molecular features such as tumor mutational load[14,15,17,26], clonal neo-antigen load[27], HLA genotype[28,29], immune infiltration into the tumor microenvironment[30], $CD8^+$ T cell activation[15,31], and expression of immune checkpoint molecules[31,32], have been correlated with response to immune checkpoint blockade.

These features have not been well described in SGCs. As clinical research expands beyond checkpoint inhibitor monotherapy, there is a clinical need to better define patients likely to benefit, and to characterize the mechanisms used by different cancer types to evade immune surveillance. These insights can help guide the next steps of clinical investigation. Here, we characterize the immune microenvironment and neoantigen landscape of ACC, MECA, and SDC tumors.

Materials and Methods

Patient samples

After written informed patient consent under an Institutional Review Board (IRB)-approved salivary tumor biospecimen protocol, tumor samples were prospectively obtained from patients undergoing treatment at Memorial Sloan Kettering Cancer Center: 20 ACC, 16 SDC, and 12 MECA samples immediately frozen in liquid nitrogen at the time of surgery and stored at -80ºC. An additional 28 MECA samples were obtained from existing formalin-fixed and embedded in paraffin (FFPE) blocks. Of the ACC cases, 9 were primary tumors collected at the time of surgery, and 11 were biopsies of metastatic sites. Two pairs of ACCs were matched primary and metastatic tumors from two individual patients (ACC_P3 and ACC_M3; ACC_P12 and ACC_M12). All MECA and SDC cases were primary tumors.

Publicly available RNAseq data from 10 different cohorts of The Cancer Genome Atlas (TCGA, https://portal.gdc.cancer.gov/) dataset were used for a comparison of tumor immune microenvironment with the SGC samples: bladder urothelial carcinoma (BLCA, n=95), breast cancer (BRCA, n=1205), colorectal adenocarcinoma (COADREAD, n=336), glioblastoma multiforme (n=123), head and neck squamous cell carcinoma (HNSC, n=293), kidney renal clear cell carcinoma (KIRC, n=658), lung adenocarcinoma (n=228), lung squamous cell carcinoma (LUSC, n=258), ovarian serous cystadenocarcinoma (OV, n=248), uterine corpus endometrial carcinoma (UCEC, n=534).

All studies were conducted in accordance with the Declaration of Helsinki and the International Ethical Guidelines for Biomedical Research Involving Human Subjects (CIOMS) and were approved by an Institutional Review Board (IRB). Written informed consent was obtained from all study participants.

Immunohistochemistry (IHC)

Formalin-fixed paraffin-embedded (FFPE) tissue sections of ACC, SDC and MECA tumors were sectioned onto glass slides at 4 µm thickness and consecutive tissue sections were stained with antibodies using Discovery XT processor (Ventana

Medical Systems). Hematoxylin and eosin (H&E) stains were performed under standard procedures and reviewed by a salivary and head and neck pathologist (N.K.) to confirm the histological diagnosis and evaluate additional immunostaining.

For IHC, tissue sections were deparaffinized with EZPrep buffer (Ventana Medical Systems), antigen retrieval was performed with CC1 buffer (Ventana Medical Systems) and sections were blocked for 30 min with Background Buster solution (Innovex), followed by avidin-biotin blocking (Ventana Medical Systems) for 8 min. Anti-CD45 (DAKO, cat# M0701, 0.5 µg/ml), anti-PD-1 (Ventana, cat# 760-4895, 3.1 µg/ml), anti-CD3 (DAKO, cat# A0452, 1.2 µg/ml), or anti-PD-L1 (Cell Signaling, cat#13684, 5 µg/ml) antibodies were applied and sections were incubated for 5 hours, followed by a 60 min incubation with biotinylated horse anti-mouse IgG (Vector labs cat# MKB-2225B) for CD45 and PD-1 antibodies, or goat anti-rabbit IgG (Vector labs, cat#PK6101) for CD3 and PD-L1 antibodies at 1:200 dilution in 3%(w/v) BSA-PBS. The detection was performed with a DAB detection kit (Ventana Medical Systems) according to the manufacturer's instructions. Slides were counterstained with hematoxylin and enclosed in a coverslip with Permount cover medium (Fisher Scientific).

Quantification of stained slides was performed manually by a head and neck/salivary pathologist blinded to the IIS and TIS values per sample by counting the number of positive leukocytes in the central region of the tumor under 400X magnification. The fields were chosen randomly in the central region of the tumor presupposing a tumor portion of at least 80%. In total, positively stained leukocytes were counted in 10 fields per section and the arithmetic mean was used for statistics.

RNA sequencing

RNA was extracted with either the RNeasy Plus Mini Kit (Qiagen) or RNeasy FFPE Kit (Qiagen), and RNAseq libraries were prepared by using KAPA Stranded RNAseq with RiboErase sample preparation kit (KAPA Biosystems) using protocols for salivary cancers [8,10]. Sequencing was performed on HiSeq 2500 (Illumina) with paired-end reads of 50 (PE50) and 137M-234M reads per sample (SDCs), 104M-194M reads per sample (MECA frozen), 92M-400M reads per sample (MECA FFPE) and 170M-321M reads per sample (ACC).

DNA extraction and whole exome sequencing (WES)

DNA was extracted using the Blood and Tissue Kit (Qiagen). DNA quality and integrity was then analyzed using BioAnalyzer (Agilent Technologies). WES libraries were prepared with the SureSelectXT Library Preparation Kit (Agilent) according to the manufacturer's instructions. Extracted DNA was then sheared using an LE220 Focus-ultrasonicator (Covaris), and the fragments were end-repaired, adenylated, ligated to Illumina sequencing adapters, and amplified by PCR. Exome capture was performed using the SureSelectXT v4 51 Mb capture probe set (Agilent), and captured exome libraries were then enriched by PCR. Final libraries were quantified with the KAPA Library Quantification Kit (KAPA Biosystems), Qubit Fluorometer (Life Technologies), and 2100 BioAnalyzer (Agilent) and were sequenced on a HiSeq2500 sequencer (Illumina) using 2 × 125 bp cycles as previously described[8]. Tumor mutational burden was calculated as the number of coding mutations per megabase, also incorporating additional exome data from previously published WES samples from our laboratory analyzed using the same mutation calling algorithm[5,8,10].

Gene expression analyses

RNAseq raw read sequences were aligned against human genome assembly hg19 by STAR 2-pass alignment. Gene level count values were computed by the summarizeOverlaps function from the R package "GenomicAlignments" with hg19 KnownGene as the base gene model. The Union counting mode was used and only mapped paired reads were considered. FPKM (Fragments Per Kilobase Million) values were then computed from gene level counts by using FPKM function from the R package "DESeq2." After principal components analysis to visualize possible batch effects, the ComBat batch correction method was used[33] through implementation in R sva package [34].

Immune infiltration and immune activity analyses

A set of previously published, orthogonal tools for assessing immune infiltration and activity in tumors using bulk RNAseq data were applied. Cell-type Identification by

Estimating Relative Subsets of RNA Transcripts (CIBERSORT) uses a reference gene expression signature and performs a linear support vector regression to adaptively select genes from the reference[35]. Single-Sample Gene Set Enrichment Analysis (ssGSEA)[36] calculates enrichment scores for a sample and gene set pair, allowing clustering by pathways rather than individual genes, and generates metrics for individual cell populations as well as aggregate measures of immune infiltration (IIS) and T cell infiltration (TIS) scores[37]. IIS is an aggregate score for innate and adaptive immune scores, while TIS is an aggregate score of nine T cell subtypes. Estimation of Stromal and Immune Cells in Malignant Tumor Tissues using Expression Data (ESTIMATE) is an ssGSEA-based technique, in which differential gene expression from high and low immune cell infiltrating tumor samples is used to derive a 141-gene signature estimating the degree of stromal and immune infiltration in a tumor[38]. Immune cytolytic activity ("CYT" score) is calculated from geometric means of transcript levels of the two effector genes granzyme A (GZMA) and perforin (PRF1) [39]. Batch-corrected normalized data were used for input into TIDE (Tumor Immune Dysfunction and Exclusion) [40].

Differentially expressed gene and pathway analysis

Five tumor samples with the highest and the lowest IIS per SGC histology were used for differentially expressed gene (DEG) analysis with the DESeq2 package in R. Given the raw count data and gene model used, DESeq2 normalized the expression raw count data by sample specific size factor while testing for genes found with significantly different expression between the high IIS group and the low IIS group samples. Qiagen Ingenuity Pathway Analysis (IPA) was used for canonical pathway analysis of differentially expressed genes, with Benjamini-Hochberg false discovery rate correction.

Mutation-associated and fusion neo-antigen identification and HLA affinity prediction

Mutation-associated neo-epitopes were identified and binding to HLA was predicted by NetMHCpan 4.0[41], with patient-specific HLA type determined using PolySolver[42]. Fusion-derived neo-antigens and binding to HLA were predicted using

INTEGRATE-Neo, which identifies two gene spanning (i.e. gene fusion) transcripts and HLA type based on RNAseq data and predicts binding using NetMHC[43]. HLA zygosity and allele-specific copy number analyses were performed using FACETS [44]. Mutational data from exome sequencing was available for all 16 SDC samples, 9 ACCs and 12 MECAs (total n = 37).

Statistical analyses

D'Agostino & Pearson omnibus normality test was performed to determine if datasets follow a Gaussian distribution in each comparison. If the data was Gaussian, parametric tests were performed (two-tailed unpaired t-tests, one-way ANOVA with Tukey's correction for multiple comparisons, or Pearson correlation). If the data was non-Gaussian, non-parametric tests were applied (Mann-Whitney-U test, one-way ANOVA using Kruskal-Wallis with Dunn's correction for multiple comparisons, or Spearman correlation). The a priori definition of statistical significance for all hypothesis testing was two-tailed $\alpha<.05$. The test used is specified in each figure or table.

Results

Deconvolution of immune infiltration and activity in SGCs

A cohort of 76 salivary gland tumors from patients undergoing treatment at Memorial Sloan Kettering Cancer Center (MSKCC, New York, USA) was analyzed for this study: 20 ACCs, 40 MECAs, and 16 SDCs. Median followup time was 41.5 months. The clinical and pathological features including treatment modalities and past medical history are shown in **Table 1** and **Supplementary Table S1**. Tumors underwent RNA sequencing (RNAseq) and normalized data were analyzed to quantify and deconvolve immune infiltration using several methods, including CIBERSORT[35], ESTIMATE[38], single sample gene set enrichment analysis (ssGSEA)[37], and cytolytic (CYT) score[39] (Supplementary Table S1).

To place salivary cancer immunity in context, we compared the immune infiltration observed in SGCs to 10 other cancer types. ACCs and MECAs consistently exhibited comparatively immune-depleted microenvironments. On the other hand, SDCs were generally more highly immune infiltrated, comparable to levels observed in clear cell kidney cancer and non-small cell lung carcinoma (**Figure 1A**).

Immune cell infiltration and somatic tumor mutational burden (TMB) are complementary measures that together provide information predictive of response to immune checkpoint inhibitor therapy[45], by reflecting aspects of both immunity and neoantigen landscape. Compared to the other cancer types, ACC and MECA tumors generally had low levels of both immune infiltration and TMB. In contrast, SDCs had much higher TMB and immune infiltration levels, although levels were moderate in comparison to other cancer types (**Figure 1B, C**). We found no significant correlations between immune infiltration and patient age, sex or autoimmune disease history.

The 76 SGC samples were then individually compared by performing unsupervised hierarchical clustering of the tumors based on immune deconvolution derived from these 4 methods, revealing an immune-poor cluster and an immune-rich cluster (**Figure 2A**). Nearly all SDC tumors (15 of 16, 94%) were in the immune-rich cluster. In contrast, most of the ACCs (16 of 20, 80%) were in the immune-poor cluster, while MECAs were more broadly distributed across both clusters.

Among the three SGC histologies, SDCs generally had a significantly higher level of T-cell inflammation (TIS) and T cell cytolytic activity (CYT score), compared with ACCs and MECAs (p≤.001 for both metrics, SDC vs ACC or MECA, **Figure 2B, C**). Identical results were observed for other immunity metrics (IIS, ESTIMATE Immune Score, and CIBERSORT; p≤.01 for all comparisons, **Supplementary Figure S1A-C**).

Comparison of RNAseq-derived and IHC-derived immunophenotyping

To determine whether these RNAseq-derived metrics of tumor immunity were consistent with one another, and with histologic assessment of immune cell infiltration in salivary tumors, we systematically examined the inter-method agreement of each of these techniques.

In the analyzed salivary tumors, the RNAseq-derived immune metrics (CIBERSORT, ESTIMATE, CYT, and ssGSEA) were strongly correlated with one another (Spearman r=.73-.95, p<.0001, **Supplementary Figure S2**). In 16 representative cases with sufficient tissue available for immunohistochemistry (IHC) analysis, IHC staining targeting CD45 and CD3 including respective negative controls (mouse-IgG and rabbit-IgG) was performed. We found that IHC-derived and RNAseq-derived measures of leukocyte infiltration (CD45+ cells, IIS) were strongly correlated (Spearman r=.67, p=.005), as were measures of T-cell infiltration (CD3+ cells , TIS; Spearman r=.63, p=.008) (**Supplementary Figure S3; Supplementary Table S2**) demonstrating a high validity of RNAseq. These correlations indicate that, in SGC tumors, RNAseq-derived deconvolution techniques measure aspects of the tumor immune microenvironment in a manner that is consistent and reproducible, and representative of leukocyte infiltration observable with IHC.

Infiltrating immune cellular populations and checkpoints

RNAseq data were analyzed to deconvolve the levels of individual immune cell populations, antigen presentation machinery, and T cell checkpoints. As with the aggregate scores, SDCs tended to have the highest levels, and ACCs the lowest levels, of individual immune cell populations including NK cells, CD8+ T cells, Th17 cells, follicular T helper cells, Th2 cells, Treg cells, Th1, cells, activated and inactivated

dendritic cells, B cells, mast cells, neutrophils, macrophages, eosinophils, gamma delta T cells, central memory T cells, and effector memory T cells (**Figure 3A).** In **Supplementary Figure S4**, immune cell subpopulations were analyzed in more detail showing a similar trend with the highest immune cell levels in SDC and the lowest in ACC. Comparable results were observed for measures of the activity of antigen processing/presenting machinery (APM1 and APM2, quantified with ssGSEA, **Figures 3A-B**). The APM Score is determined by seven genes: *HLA-A/B/C*, *B2M*, *TAP1*, *TAP2*, and *TAPBP*[37]. APM score was strongly correlated with T cell infiltration (Spearman r=.84, p<.0001; **Figure 3B**), consistent with the ability of $CD8^+$ T cells to upregulate the expression of APM through secretion of IFNγ, and was highest in SDCs, compared to ACCs and MECAs. Examining the combination of mutational load and antigen presentation, we found that ACCs had the lowest of each measure, indicating that these tumors have profoundly low levels of tumor antigen availability and presentation (**Supplementary Figure S5**).

Highly T-cell infiltrated cancers are often able to escape immune surveillance because the constituent T cells are in a dysfunctional or exhausted state. We therefore examined the expression of T cell checkpoints PD-1 (and its ligand PD-L1), CTLA-4, LAG3, TIM3, TIGIT, and VISTA (*VSIR*) in immune-high vs immune-low SGCs, and across histologies. We found that all of these checkpoints were expressed at significantly higher levels in immune-rich salivary tumors, compared to immune-poor tumors: the most significant differences were in PD1, CTLA4, LAG3, TIM3, and TIGIT expression (**Supplementary Figure S6**). Delineated for the three different histologies, SDCs had much higher expression of these T cell checkpoints than ACCs and MECAs (**Figure 3A and Supplementary Figure S7**). We also used an orthogonal measure of T cell dysfunction, TIDE (Tumor Immune Dysfunction and Exhaustion), which uses a distinct gene signature including *TGFB1, SOX10*, and other genes independently discovered to modulate the effect of T cell activity on clinical outcome[40]. Again, we found that SDCs had much higher levels of T cell dysfunction than MECA or ACC (all p<.01; **Figure 3D**).

More immune-depleted tumors may instead achieve immune evasion by excluding T cells. To examine these possible mechanisms in SGCs, we used TIDE to

analyze transcriptome-based gene signatures of T cell exclusion. We found that immune-poor SGCs had significantly higher T cell exclusion scores (p=.0002), associated with higher levels of myeloid-derived suppressor cells (MDSCs; p<.0001) and of M2-polarized tumor-associated macrophages (p<.0001) (**Supplementary Figure S8A-C**). This phenotype was seen most clearly in ACCs (**Supplementary Figure S9**), which demonstrated higher levels of MDSC and M2 macrophage infiltration (**Figure 3E-F**), compared to MECA and SDC. While T cell exclusion did not significantly differ depending on histology, significant differences were found for MDSC and M2 macrophage infiltration, with the highest levels in ACC (**Supplementary Figure S8D-F**).

These data reveal several key immune evasion mechanisms at play in salivary tumors. SDCs have high neoantigen load and are highly immune infiltrated, but T cells are characterized by high levels of dysfunction. At the other end of the spectrum, ACCs are characterized by very low neoantigen load, a T cell exclusion phenotype, and a microenvironment comprised of more immunosuppressive MDSCs and M2 macrophages. MECAs are more heterogeneous, representing the entire spectrum of immunity, with more intermediate mutational load.

Immune infiltration correlates with aggressive clinical behavior

To determine whether the level of T cell infiltration in the tumor microenvironment was associated with clinical outcome, we compared SGCs that ultimately developed recurrence (either locoregional or distant), and those that did not recur. We found that recurrent/metastatic SGCs had a significantly lower level of T cell infiltration compared with non-recurrent/metastatic cases (p=.02, **Figure 4A**). When samples were stratified by histology, the relationship was observed in ACCs (p=.008) and MECAs (p=.005), but not in SDCs (p=.31). Similar results were observed when these comparisons were made with IIS instead (**Supplementary Figure S10**).

These data lead us to hypothesize that lack of immune surveillance, as evidenced by an immune-poor microenvironment, may be associated with the ability of ACC and MECA tumors to develop recurrence or distant metastasis after initially definitive therapy. It is important to clarify that in view of the small number of tumors analyzed, these findings are hypothesis-generating. However, a similar association

between T cell infiltration and tumor recurrence was recently observed in ACC by Mosconi and colleagues[46]. In our study, this association was not observed in SDCs, perhaps because there were very few SDCs as immune-depleted as the ACCs and MECAs. SDCs that recur or metastasize may utilize other means of immune evasion, although there were no differences in engagement of T cell checkpoints, T cell dysfunction, exclusion, or immunosuppressive cell populations in those SDCs developing recurrence.

We also examined the association of immunity with the evolution of carcinomas from benign adenomas. Salivary carcinomas with particularly aggressive behavior can arise from longstanding benign pleomorphic adenomas of the salivary glands, termed "carcinoma ex pleomorphic adenoma" (ex-PA). SDCs and MECAs are the 2 most common malignant histologies that develop ex-PA.

In this cohort, 6 of 16 SDCs (37.5%) and 24 of 40 MECAs (60%) had arisen from a pre-existing pleomorphic adenoma. We observed that SDCs ex-PA had a significantly lower IIS and TIS than SDCs *de novo* (p=.04 and p=.03, respectively; **Supplementary Figure S11A-B**). This difference was mainly driven by lower levels of CD8+ T cells in SDCs ex-PA (p=.04; **Supplementary Figure S12**). In MECA, while IIS and TIS were numerically lower in ex-PA cancers, these differences were not statistically significant (p=.09 and p=.11, respectively; **Supplementary Figure S11C-D**).

In these exploratory analyses, we observed that a relative lack of immune surveillance appeared to be associated with more aggressive tumor behavior – the development of tumor recurrence/metastasis in ACCs and MECAs, or the development of a carcinoma from a benign adenoma in SDCs. Further immunophenotyping of salivary cancers and benign tumors will help to elucidate these relationships.

Canonical pathways involved in differentially immune-infiltrated SGCs

We then examined the transcriptional programs that were differentially activated between immune-rich and the immune-poor tumors (as depicted in **Figure 2A**). The transcriptomes from samples with the highest and the lowest IIS values were compared within each of the three SGC histologies. Ingenuity Pathway Analysis (IPA, Qiagen) of significantly differentially expressed genes was used to identify enriched canonical

pathways. Among the pathways that were significantly enriched between immune-high and immune-low tumors, 7 pathways were consistently enriched in all 3 SGC histologies (**Figure 4C**), including Th1 and Th2 pathways, IL-4 signaling, B cell signaling, and inducible co-stimulator (iCOS) signaling in T helper cells. Although these immune pathways were significantly enriched among immune-rich tumors in all 3 histologies, the degree of enrichment (as measured by $-\log_{10}$ p-value) was much higher in SDC and MECA compared to ACC, indicating that the natural range of immunity in ACC tumors is fairly narrow (**Figure 4D**). These findings expand upon the phenotypes revealed by RNAseq deconvolution of enriched immune and T cell infiltration and activation, and suggest that, in addition, CD4+ T cell activity and Th2 immune responses may have additional relevance to the immune-poor and immune-rich SGC subsets.

Neoantigen landscape and HLA loss

In 36 cases (8 ACC, 12 MECA, 16 SDC) with additional exome sequencing available, somatic mutations and mutation-derived neoantigens predicted to bind to patient-specific HLA class I, were identified using netMHCpan (**Supplementary Tables S3-5**). Gene fusions can also generate immunogenic neoantigens[47]. Gene fusions are particularly prevalent in salivary carcinomas, and represent common oncogenic alterations in ACC and MECA. Analysis of RNAseq data in SGCs identified fusion-derived neoantigens predicted to bind patient-specific HLA class I in 49 cases (19 ACC, 14 MECA, and 16 SDC) (**Supplementary Tables S6-8**). SNV- and fusion-associated neoantigen counts are summarized per sample in **Supplementary Table S9**. As expected, the number of neoantigens generated by missense mutations (single nucleotide variant neoantigens, SNV-NeoAg) was tightly correlated with the number of SNVs in the tumor (Spearman r=.82, p<.0001; **Supplementary Figure S5**). SDCs had the highest, and ACCs the lowest, level of SNV-NeoAg (p=.002). Numbers of fusion-derived neoantigens (Fusion-NeoAg) tended to be lower than SNV-Neoag counts. SDCs had the highest, and MECAs the lowest, fusion neoantigen counts (p=.02; **Figure 5A**).

We analyzed associations between neoantigen landscape and the immune microenvironment. SNV load was correlated with T cell (Spearman r=.48, p=.003,

Figure 5B) and immune (Spearman r=.52, p=.001) infiltration. Predicted SNV-NeoAg abundance had a similar although slightly attenuated correlation with TIS (Spearman r=.32, p=.052, **Figure 5C**) and IIS (Spearman r=.34, p=.039, **Supplementary Figure S5B**). Because both SNV count and immune infiltration vary by histology, we performed multivariable analyses to examine the association between SNV-neoantigen count and immunity metrics, with adjustment for tumor histology. The association between SNV-Neoantigen count and the ESTIMATE immune, CYT, IIS, and TIS scores remained significant, independent of tumor histology (β>.35, p<.02 for all regression models, **Supplementary Table S10**).

Similar associations were observed between fusion neoantigen count and immune infiltration (**Figure 5D**), with the strongest association seen within the ACC tumors (**Supplementary Figure S5**). These associations demonstrate that, among these SGC histologies, which harbor very low (ACC, MECA), or moderate (SDC) mutational load, that the degree of immune infiltration in the tumor microenvironment does appear to correlate with the abundance of neoantigens that derive either from mutations or gene fusions. This suggests that the neoantigen landscape of these tumors impacts immune surveillance, and that for those tumors with very few neoantigens, there is a minimal pre-existing anti-tumor immune response.

For these reasons, salivary cancers with low mutational load and, consequently, low neoantigen load, which also have the least inflamed tumor microenvironments, appear to be the least poised to respond to immune checkpoint inhibitors, at least as monotherapy.

Finally, we examined whether SGCs utilize loss of HLA, which would impair the ability to present a diverse neoantigen repertoire, as a means of immune evasion. Using FACETS[44] to call allele-specific copy number at the HLA class I locus in each case with exome sequencing of normal DNA, we determined which cases harbored either single-copy loss of HLA (hemizygous or copy-neutral loss of heterozygosity) or at least one homozygous HLA class I allele[29]. This analysis revealed that HLA LOH/homozygosity was prevalent in ACC (44%) and SDC (31%) tumors, but uncommon in MECAs (8%; **Supplementary Figure S13**). We hypothesize that certain SGC histologies, especially ACC, may employ HLA loss as an immune escape mechanism. These findings are

preliminary, and further analyses with a larger number of samples will be needed for confirmation. Because HLA status modulates response to immunotherapy in diverse cancer types, these findings may have relevance in future analyses of immunotherapy-treated SGCs.

Discussion

To further improve clinical benefit from immunotherapy, rational investigation of these drugs should ideally be guided by molecular features that reflect the likelihood of response, and the potential vulnerabilities that may be targetable with different monotherapies or combination therapies.

Here, we describe the immunity landscape of 3 types of salivary gland carcinoma – adenoid cystic (ACC), myoepithelial (MECA), and salivary duct carcinomas (SDC). These are rare, lethal malignancies that are difficult to treat, owing to a lack of active systemic therapies. Data regarding immunotherapy response are limited but thus far have suggested that response rates are low in SGCs. To address this, we performed extensive immunogenomic profiling of 76 clinically annotated salivary cancers.

We find that each of these salivary cancers differs in terms of immunologic microenvironment and likely vulnerabilities. On the one hand, SDCs have the most favorable immunogenomic profile, with moderate TMB and moderate-to-high levels of microenvironment inflammation. In contrast, ACCs have immunogenomic profiles that are less favorable for immunotherapy, with very low TMB, an immune-depleted microenvironment, and possibly a high prevalence of HLA class I loss. MECAs were more intermediate. Understanding these profiles suggests that different immunotherapeutic approaches will be needed for each of these cancer types. Checkpoint inhibitor monotherapy is unlikely to achieve high response rates in any of these cancers.

Our findings from the first comprehensive immune deconvolution of SGCs build upon, and are consistent with, prior studies using IHC or targeted gene expression techniques to describe aspects of immune infiltration in salivary tumors. Mosconi et al. analyzed 36 ACC samples by IHC, finding that no cases (0%) were PD-L1 positive, as well as comparably low levels of CD8+ and Granzyme B-positive TILs, CD1a+ and

CD83+ cell populations[46], in agreement with our observation that 80% of the ACCs in our study were in the immune-poor cluster, likely driven by a T cell exclusion phenotype. In a similar study, Chang et al. performed immunohistochemical staining of several immune markers including CD8 in 70 SGC patients and found a higher number of CD8+ T cells in SDCs and mucoepidermoid carcinomas than in ACCs [48]. Sridharan et al. performed a targeted gene expression panel in 12 ACCs and again reported a comparably low number of infiltrating immune cells [49].

Our analyses identified possible mechanisms for immune evasion in salivary cancers. In ACCs, T cell exclusion and comparably higher levels of strongly immunosuppressive MDSC and M2 macrophage populations generate a “cold” immune microenvironment. This immune-depleted microenvironment appeared clinically relevant, because it was associated with a higher likelihood of cancer recurrence in ACCs. Because T cell checkpoints were universally expressed at low levels in ACCs, and because the mutational load of ACCs is very low (0.3 mutations/megabase), indicating a paucity of tumor antigens, the therapeutic approach of inhibiting single T cell checkpoints, such as with anti-PD-1 monotherapy, is not likely to be sufficient to achieve responses in ACC. Successful immunotherapy for ACC is likely to require approaches to reverse T cell exclusion and the immunosuppressive sequelae of MDSC and M2 macrophage infiltration, perhaps leveraging emerging agents such as immune agonists, vaccines, or targeting immunosuppressive cytokines and the peritumoral stroma.

In contrast, SDCs harbor much higher levels of T cell infiltration that were associated with markedly higher levels of T cell dysfunction and high expression of T cell checkpoints. This is in agreement with prior literature reporting rates of PD-L1 positivity in SDCs of 30-60%[50]. In combination with a higher availability of tumor antigens resulting from a moderate mutational burden (1.7 mutations/megabase), these data indicate that SDCs are more poised to respond to T cell checkpoint inhibitors, although combination therapies that target multiple checkpoints may ultimately be needed.

MECAs were a more heterogeneous group of cancers, with some clustering closer to ACC and some clustering closer to SDC in terms of immune infiltration. Further investigation will be needed to determine if it is clinically helpful to profile these cancers

with measures of T cell infiltration and tumor mutational burden in order to triage them to therapy. All of these potential approaches for these cancer types will require further investigation.

Despite their lower mutational load, ACCs and MECAs do have another potential source of neoantigens: highly prevalent fusion genes, such as *MYB-NFIB* in ACC and *PLAG1* fusions in MECA. In this study, we found that fusion-derived neoantigens were associated with higher levels of T cell inflammation. We have previously shown that several patients with metastatic ACC had circulating T cells that recognize a *MYB-NFIB* fusion-associated peptide[47]. Taken together, these data suggest that fusion-derived neoantigens may represent a source of targetable tumor antigens in SGCs.

A major challenge faced by the field of salivary oncology is the rarity of these entities, and the large number of cancer histologies included under the category of "salivary cancer." These data can help to inform and prioritize immunotherapeutic research strategies for each of these cancer types. The molecular landscape of each salivary cancer histology is unique and informative. It is notable that in recent years, targeted therapies focused on specific molecular alterations in individual SGC histologies have begun to demonstrate activity, including recent trials of lenvatinib[51] and *NOTCH1*-targeted agents in ACC[52,53], and androgen receptor and Her2/*ERBB2*-targeted approaches in SDC[54,55].

Our study was necessarily limited in that we selected only the most clinically aggressive types of SGC. We did not profile less clinically aggressive SGC types such as mucoepidermoid or polymorphous adenocarcinomas. Clinical data from immune checkpoint blockade in SGCs has been limited to the KEYNOTE-028 study [25], but we await the results of a number of ongoing phase II trials enrolling more patients with SGC (KEYNOTE-158, NCT02628067; NISCAHN, NCT03132038; NCT02538510).

This study aims to provide new insights into the immune microenvironment, potential mechanisms of immune evasion, and possible vulnerabilities needing further study, in these rare, aggressive, often incurable cancers. Our data reveal that these cancer types are vastly different from one another from the standpoint of immunity. Despite the heterogeneity of SGCs, these cancers are often grouped together in the context of clinical trials. These data provide necessary information that may help to

guide the next steps of investigation, perhaps helping to prioritize or nominate certain immunotherapeutic approaches for certain SGC histologies.

Data availability

RNAseq and whole exome sequencing data for the included tumors have been uploaded to the NCBI Sequence Read Archive (SRA) under accession numbers SRP109264, SRP096726, and PRJNA601423..

Acknowledgements

We express our deep gratitude to our brave patients and their families who participated in these studies. We thank Jeffrey and Marnie Kaufman and Nicole Spardy Burr from the Adenoid Cystic Cancer Research Foundation for their support and leadership, and members of the Chan Lab for helpful discussions. We acknowledge funding from the Frederick Adler Chair (LGTM), Cycle for Survival (LGTM), the Jayme Flowers Fund (LGTM), The Sebastian Nativo Fund (LGTM), NIH K08 DE024774 and R01 DE027738 (LGTM), the Adenoid Cystic Carcinoma Research Foundation (TAC), Pershing Square Sohn Cancer Research grant (TAC), the PaineWebber Chair (TAC), Stand Up 2 Cancer (TAC), NIH R01 CA205426, the STARR Cancer Consortium (TAC), NCI R35 CA232097 (TAC), and funding to MSKCC through NIH/NCI Cancer Center Support Grant (P30 CA008748).

References

1 El-Naggar, A. K., Chan, J. K. C., Grandis, J. R., Takata, T. & Slootweg, P. J. *WHO Classification of Head and Neck Tumors.*, Vol. 4th edition (IARC Publications, 2017).
2 Alfieri, S. *et al.* Systemic therapy in metastatic salivary gland carcinomas: A pathology-driven paradigm? *Oral Oncol* **66**, 58-63, doi:10.1016/j.oraloncology.2016.12.016 (2017).
3 Laurie, S. A., Ho, A. L., Fury, M. G., Sherman, E. & Pfister, D. G. Systemic therapy in the management of metastatic or locally recurrent adenoid cystic carcinoma of the salivary glands: a systematic review. *Lancet Oncol* **12**, 815-824, doi:10.1016/S1470-2045(10)70245-X (2011).
4 Persson, M. *et al.* Recurrent fusion of MYB and NFIB transcription factor genes in carcinomas of the breast and head and neck. *Proc Natl Acad Sci U S A* **106**, 18740-18744, doi:10.1073/pnas.0909114106 (2009).
5 Ho, A. S. *et al.* The mutational landscape of adenoid cystic carcinoma. *Nat Genet* **45**, 791-798, doi:10.1038/ng.2643 (2013).
6 Ho, A. S. *et al.* Genetic hallmarks of recurrent/metastatic adenoid cystic carcinoma. *J Clin Invest*, doi:10.1172/jci128227 (2019).
7 Kane, S. V. & Bagwan, I. N. Myoepithelial carcinoma of the salivary glands: a clinicopathologic study of 51 cases in a tertiary cancer center. *Arch Otolaryngol Head Neck Surg* **136**, 702-712, doi:10.1001/archoto.2010.104 (2010).
8 Dalin, M. G. *et al.* Multi-dimensional genomic analysis of myoepithelial carcinoma identifies prevalent oncogenic gene fusions. *Nat Commun* **8**, 1197, doi:10.1038/s41467-017-01178-z (2017).
9 Jayaprakash, V. *et al.* Survival rates and prognostic factors for infiltrating salivary duct carcinoma: Analysis of 228 cases from the Surveillance, Epidemiology, and End Results database. *Head Neck* **36**, 694-701, doi:10.1002/hed.23350 (2014).
10 Dalin, M. G. *et al.* Comprehensive Molecular Characterization of Salivary Duct Carcinoma Reveals Actionable Targets and Similarity to Apocrine Breast Cancer. *Clin Cancer Res* **22**, 4623-4633, doi:10.1158/1078-0432.CCR-16-0637 (2016).
11 Di Palma, S. *et al.* Salivary duct carcinomas can be classified into luminal androgen receptor-positive, HER2 and basal-like phenotypes. *Histopathology* **61**, 629-643, doi:10.1111/j.1365-2559.2012.04252.x (2012).
12 Thorpe, L. M. *et al.* Significant and durable clinical benefit from trastuzumab in 2 patients with HER2-amplified salivary gland cancer and a review of the literature. *Head Neck* **39**, E40-E44, doi:10.1002/hed.24634 (2017).
13 Griffith, C. C., Seethala, R. R., Luvison, A., Miller, M. & Chiosea, S. I. PIK3CA mutations and PTEN loss in salivary duct carcinomas. *Am J Surg Pathol* **37**, 1201-1207, doi:10.1097/PAS.0b013e3182880d5a (2013).

14 Snyder, A. *et al.* Genetic basis for clinical response to CTLA-4 blockade in melanoma. *N Engl J Med* **371**, 2189-2199, doi:10.1056/NEJMoa1406498 (2014).
15 Van Allen, E. M. *et al.* Genomic correlates of response to CTLA-4 blockade in metastatic melanoma. *Science* **350**, 207-211, doi:10.1126/science.aad0095 (2015).
16 Weber, J. S. *et al.* Nivolumab versus chemotherapy in patients with advanced melanoma who progressed after anti-CTLA-4 treatment (CheckMate 037): a randomised, controlled, open-label, phase 3 trial. *Lancet Oncol* **16**, 375-384, doi:10.1016/S1470-2045(15)70076-8 (2015).
17 Rizvi, N. A. *et al.* Cancer immunology. Mutational landscape determines sensitivity to PD-1 blockade in non-small cell lung cancer. *Science* **348**, 124-128, doi:10.1126/science.aaa1348 (2015).
18 Brahmer, J. *et al.* Nivolumab versus Docetaxel in Advanced Squamous-Cell Non-Small-Cell Lung Cancer. *N Engl J Med* **373**, 123-135, doi:10.1056/NEJMoa1504627 (2015).
19 Reck, M. *et al.* Pembrolizumab versus Chemotherapy for PD-L1-Positive Non-Small-Cell Lung Cancer. *N Engl J Med* **375**, 1823-1833, doi:10.1056/NEJMoa1606774 (2016).
20 Motzer, R. J. *et al.* Nivolumab for Metastatic Renal Cell Carcinoma: Results of a Randomized Phase II Trial. *J Clin Oncol* **33**, 1430-1437, doi:10.1200/JCO.2014.59.0703 (2015).
21 Balar, A. V. *et al.* Atezolizumab as first-line treatment in cisplatin-ineligible patients with locally advanced and metastatic urothelial carcinoma: a single-arm, multicentre, phase 2 trial. *Lancet* **389**, 67-76, doi:10.1016/s0140-6736(16)32455-2 (2017).
22 Ferris, R. L. *et al.* Nivolumab for Recurrent Squamous-Cell Carcinoma of the Head and Neck. *N Engl J Med* **375**, 1856-1867, doi:10.1056/NEJMoa1602252 (2016).
23 Ferris, R. & Gillison, M. L. Nivolumab for Squamous-Cell Cancer of Head and Neck. *N Engl J Med* **376**, 596, doi:10.1056/NEJMc1615565 (2017).
24 Cohen, E. E. W. *et al.* Pembrolizumab versus methotrexate, docetaxel, or cetuximab for recurrent or metastatic head-and-neck squamous cell carcinoma (KEYNOTE-040): a randomised, open-label, phase 3 study. *Lancet* **393**, 156-167, doi:10.1016/s0140-6736(18)31999-8 (2019).
25 Cohen, R. B. *et al.* Pembrolizumab for the Treatment of Advanced Salivary Gland Carcinoma: Findings of the Phase 1b KEYNOTE-028 Study. *Am J Clin Oncol*, doi:10.1097/coc.0000000000000429 (2018).
26 Samstein, R. M., Lee, C. H. & Shoushtari, A. N. Tumor mutational load predicts survival after immunotherapy across multiple cancer types. **51**, 202-206, doi:10.1038/s41588-018-0312-8 (2019).
27 McGranahan, N. *et al.* Clonal neoantigens elicit T cell immunoreactivity and sensitivity to immune checkpoint blockade. *Science* **351**, 1463-1469, doi:10.1126/science.aaf1490 (2016).
28 McGranahan, N. *et al.* Allele-Specific HLA Loss and Immune Escape in Lung Cancer Evolution. *Cell* **171**, 1259-1271.e1211, doi:10.1016/j.cell.2017.10.001 (2017).
29 Chowell, D. & Morris, L. G. T. Patient HLA class I genotype influences cancer response to checkpoint blockade immunotherapy. **359**, 582-587, doi:10.1126/science.aao4572 (2018).
30 Gajewski, T. F., Schreiber, H. & Fu, Y. X. Innate and adaptive immune cells in the tumor microenvironment. *Nat Immunol* **14**, 1014-1022, doi:10.1038/ni.2703 (2013).

31 Tumeh, P. C. *et al.* PD-1 blockade induces responses by inhibiting adaptive immune resistance. *Nature* **515**, 568-571, doi:10.1038/nature13954 (2014).
32 Topalian, S. L. *et al.* Safety, activity, and immune correlates of anti-PD-1 antibody in cancer. *N Engl J Med* **366**, 2443-2454, doi:10.1056/NEJMoa1200690 (2012).
33 Johnson, W. E., Li, C. & Rabinovic, A. Adjusting batch effects in microarray expression data using empirical Bayes methods. *Biostatistics* **8**, 118-127, doi:10.1093/biostatistics/kxj037 (2007).
34 Parker, H. S. *et al.* Preserving biological heterogeneity with a permuted surrogate variable analysis for genomics batch correction. *Bioinformatics (Oxford, England)* **30**, 2757-2763, doi:10.1093/bioinformatics/btu375 (2014).
35 Newman, A. M. *et al.* Robust enumeration of cell subsets from tissue expression profiles. *Nat Methods* **12**, 453-457, doi:10.1038/nmeth.3337 (2015).
36 Subramanian, A. *et al.* Gene set enrichment analysis: a knowledge-based approach for interpreting genome-wide expression profiles. *Proc Natl Acad Sci U S A* **102**, 15545-15550, doi:10.1073/pnas.0506580102 (2005).
37 Senbabaoglu, Y. *et al.* Tumor immune microenvironment characterization in clear cell renal cell carcinoma identifies prognostic and immunotherapeutically relevant messenger RNA signatures. *Genome Biol* **17**, 231, doi:10.1186/s13059-016-1092-z (2016).
38 Yoshihara, K. *et al.* Inferring tumour purity and stromal and immune cell admixture from expression data. *Nat Commun* **4**, 2612, doi:10.1038/ncomms3612 (2013).
39 Rooney, M. S., Shukla, S. A., Wu, C. J., Getz, G. & Hacohen, N. Molecular and genetic properties of tumors associated with local immune cytolytic activity. *Cell* **160**, 48-61, doi:10.1016/j.cell.2014.12.033 (2015).
40 Jiang, P. *et al.* Signatures of T cell dysfunction and exclusion predict cancer immunotherapy response. *Nat Med* **24**, 1550-1558, doi:10.1038/s41591-018-0136-1 (2018).
41 Jurtz, V. & Paul, S. NetMHCpan-4.0: Improved Peptide-MHC Class I Interaction Predictions Integrating Eluted Ligand and Peptide Binding Affinity Data. **199**, 3360-3368, doi:10.4049/jimmunol.1700893 (2017).
42 Shukla, S. A. *et al.* Comprehensive analysis of cancer-associated somatic mutations in class I HLA genes. *Nat Biotechnol* **33**, 1152-1158, doi:10.1038/nbt.3344 (2015).
43 Andreatta, M. & Nielsen, M. Gapped sequence alignment using artificial neural networks: application to the MHC class I system. *Bioinformatics (Oxford, England)* **32**, 511-517, doi:10.1093/bioinformatics/btv639 (2016).
44 Shen, R. & Seshan, V. E. FACETS: allele-specific copy number and clonal heterogeneity analysis tool for high-throughput DNA sequencing. *Nucleic Acids Res* **44**, e131, doi:10.1093/nar/gkw520 (2016).
45 Cristescu, R. *et al.* Pan-tumor genomic biomarkers for PD-1 checkpoint blockade-based immunotherapy. **362**, doi:10.1126/science.aar3593 (2018).
46 Mosconi, C. *et al.* Immune microenvironment and evasion mechanisms in adenoid cystic carcinomas of salivary glands. *Oral Oncol* **88**, 95-101, doi:10.1016/j.oraloncology.2018.11.028 (2019).
47 Yang, W. & Lee, K. W. Immunogenic neoantigens derived from gene fusions stimulate T cell responses. **25**, 767-775, doi:10.1038/s41591-019-0434-2 (2019).

48 Chang, H. *et al.* Overexpression of PD-L2 is associated with shorter relapse-free survival in patients with malignant salivary gland tumors. *Onco Targets Ther* **10**, 2983-2992, doi:10.2147/ott.s134589 (2017).
49 Sridharan, V. *et al.* Immune Profiling of Adenoid Cystic Carcinoma: PD-L2 Expression and Associations with Tumor-Infiltrating Lymphocytes. *Cancer Immunol Res* **4**, 679-687, doi:10.1158/2326-6066.cir-16-0031 (2016).
50 Xu, B. *et al.* The immune microenvironment and expression of PD-L1, PD-1, PRAME and MHC I in salivary duct carcinoma. *Histopathology*, doi:10.1111/his.13944 (2019).
51 Tchekmedyian, V. *et al.* Phase II Study of Lenvatinib in Patients With Progressive, Recurrent or Metastatic Adenoid Cystic Carcinoma. *J Clin Oncol* **37**, 1529-1537, doi:10.1200/jco.18.01859 (2019).
52 Even, C. *et al.* Safety and clinical activity of the Notch inhibitor, crenigacestat (LY3039478), in an open-label phase I trial expansion cohort of advanced or metastatic adenoid cystic carcinoma. *Invest New Drugs*, doi:10.1007/s10637-019-00739-x (2019).
53 Ferrarotto, R. *et al.* A phase I dose-escalation and dose-expansion study of brontictuzumab in subjects with selected solid tumors. *Ann Oncol* **29**, 1561-1568, doi:10.1093/annonc/mdy171 (2018).
54 van Boxtel, W. *et al.* Prediction of clinical benefit from androgen deprivation therapy in salivary duct carcinoma patients. *Int J Cancer*, doi:10.1002/ijc.32795 (2019).
55 Takahashi, H. *et al.* Phase II Trial of Trastuzumab and Docetaxel in Patients With Human Epidermal Growth Factor Receptor 2-Positive Salivary Duct Carcinoma. *J Clin Oncol* **37**, 125-134, doi:10.1200/jco.18.00545 (2019).

Table 1 - The clinical and pathological characteristics of salivary tumors obtained from patients. Note that there are two pairs of ACC cases that are matched primary and metastatic tumors from the same respective patients.

	ACC	MECA	SDC
Tumors	20	40	16
Patients	18	40	16
Male	9 (50%)	15 (38%)	12 (75%)
Female	9 (50%)	25 (63%)	4 (25%)
Median age at diagnosis (range)	63 (43-91)	69 (35-94)	63 (47-76)
Smoking history	9 (50%)	18 (45%)	10 (63%)
Primary tumor site			
Parotid gland	4 (22%)	33 (83%)	15 (94%)
Submandibular gland	2 (11%)	2 (5%)	1 (6%)
Sublingual gland	4 (22%)	0	0
Minor salivary glands	10 (56%)	5 (13%)	0
Tumor sequenced			
Primary	9 (45%)	40 (100%)	16 (100%)
Metastasis	11 (55%)	0	0
Adjuvant therapy			
None	3 (17%)	24 (60%)	1 (6%)
Radiation therapy	13 (72%)	16 (40%)	10 (63%)
Chemoradiation therapy	2 (11%)	0	5 (31%)
Recurrence			
None	4 (22%)	21 (53%)	6 (38%)
Locoregional	0	10 (25%)	1 (6%)
Distant	11 (61%)	3 (8%)	7 (44%)
Locoregional and distant	3 (17%)	6 (15%)	2 (13%)
Immunotherapy treatment	1 (5%)	0	0
Outcome			
Alive without disease	2 (11%)	25 (63%)	4 (25%)

Alive with disease	12 (67%)	2 (5%)	2 (13%)
Dead of disease	4 (22%)	9 (23%)	8 (50%)
Dead of other causes	0	4 (10%)	2 (13%)

Figure legends

Figure 1 – Immune infiltration, cytolytic activity, and TMB in SGCs compared with 10 TCGA cohorts. (A) ESTIMATE Immune Score for ACC, MEC, and SDC compared with UCEC, COADREAD, BLCA, OV, GBM, HNSC, LUAD, BRCA, and KIRC TCGA samples, representing overall immune infiltration, based on either reads per kilobase million (RPKM, RNAseq, red columns) or RSEM software analysis (RNAseqV2, green columns) of respective RNAseq data. Box and whisker blots are used to indicate T cell infiltration score for each histological subtype. Each box represents the range from the first quartile to the third quartile. The median is indicated by a line. The whiskers outside the boxes represent the ranges from the minimum to the maximum value of each group. Each dot represents one patient sample. (B) Scatterplot showing the landscape of CYT scores and tumor mutational burden (TMB), indicated as mutations per megabase, across different cancers. (C) Scatterplot showing the landscape of IIS and TMB across different cancers.

Figure 2 – Unsupervised hierarchical clustering of salivary gland cancers by aggregate immunity metrics reveals an "immune-rich" group and an "immune-poor" group. (A) RNAseq data from 76 salivary gland cancer tumors were analyzed by orthogonal immune deconvolution algorithms and the samples color-coded according to each measure. Clustering of the samples indicates that SDCs have relatively higher immune infiltration and cytolytic activity compared to ACCs and MECAs. (B) TIS and (C) log CYT Score for ACC primary tumors, ACC metastases, MECA, and SDC. In (B) and (C), box and whisker blots are used to indicate the TIS for each histological subtype. Each box represents the range from the first quartile to the third quartile. The median is indicated by a line. The whiskers outside the boxes represent the ranges from the minimum to the maximum value of each group. Statistics in B and C: Kruskal-Wallis test with Dunn's correction (non-parametric).

Figure 3 – Unsupervised hierarchical clustering of salivary gland cancers by 23 immune cell populations, checkpoint expression, and antigen processing/presenting machinery (APM). (A) RNAseq data from 76 SGC tumors were analyzed by the ssGSEA deconvolution algorithm. Clustering of the samples reveals that SDCs have overall a relatively higher infiltration with nearly all immune cell subpopulations as well as a higher expression level of T cell checkpoints. (B) Correlation of TIS and APM Score. In (C), medians and inter-quartile ranges of APM score are shown for primary ACC, ACC metastases, MECA, and SDC. TIDE was used to analyze T cell dysfunction (D), MDSC (E), and TAM M2 (F), depending on histology. MDSC – myeloid derived suppressor cells; TAM M2 – tumor associated M2 macrophages. Statistics in B: Spearman correlation (non-parametric); Statistics in D-F: Kruskal-Wallis test with Dunn's correction (non-parametric).

Figure 4 – Clinical and mechanistic differences between immune-high and immune-low salivary cancers. Comparison of T cell infiltration (TIS score) for recurrent and non-recurrent SGCs (A), with stratification by histological subtype (B). (C) Enriched canonical pathways based on differentially expressed genes in immune infiltration (IIS)-high vs. IIS-low salivary cancers is shown with a Venn diagram of enriched pathways in each of the three salivary cancer types. (D) Significance of 7 enriched pathways common to all three salivary cancer types. In (A), medians and inter-quartile ranges are shown. In (B), box and whisker blots are used to indicate the T cell infiltration score for each histological subtype. Each box represents the range from the first quartile to the third quartile. The median is indicated by a line. The whiskers outside the boxes represent the ranges from the minimum to the maximum value of each group. Statistics in A-B: Mann-Whitney U test (non-parametric); Statistics in D: Fisher exact test, Benjamini-Hochberg false discovery rate correction.

Figure 5 –SNV-NeoAg counts and Fusion-NeoAg counts depending on histology (A). (B) Correlation of TIS and SNV count (B), TIS and SNV-NeoAg count (C), TIS and Fusion-NeoAG count (D). In (A), medians and inter-quartile ranges of SNV NeoAg and Fusion NeoAg count are shown for ACC, MECA, and SDC. Statistics in A: Kruskal-Wallis test with Dunn's correction (non-parametric); Statistics in B-D: Spearman correlation.

Author Manuscript Published OnlineFirst on February 14, 2020; DOI: 10.1158/1078-0432.CCR-19-3758
Author manuscripts have been peer reviewed and accepted for publication but have not yet been edited.

Figure 5

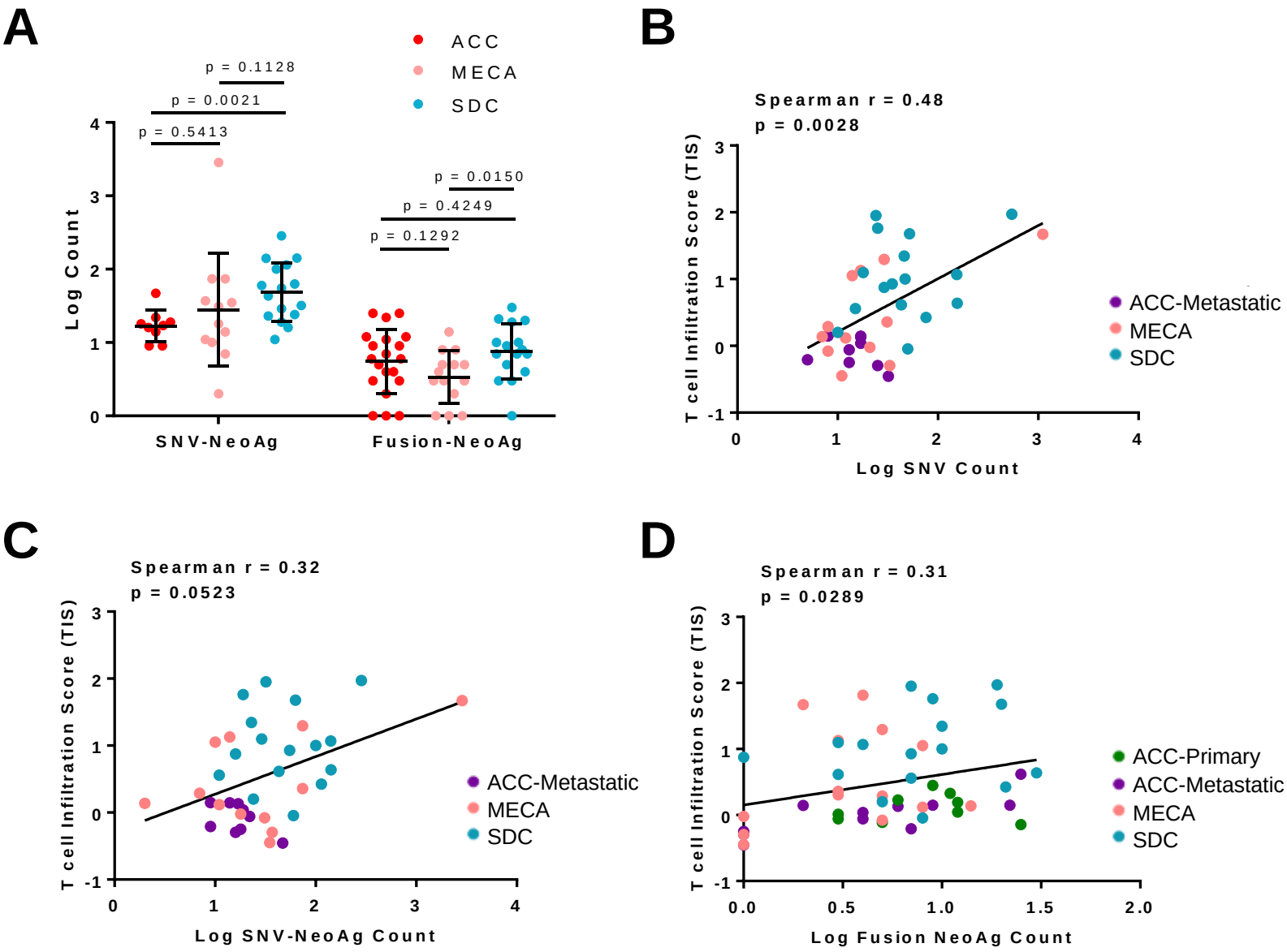

Author Manuscript Published OnlineFirst on February 14, 2020; DOI: 10.1158/1078-0432.CCR-19-3758
Author manuscripts have been peer reviewed and accepted for publication but have not yet been edited.

Figure 4

A

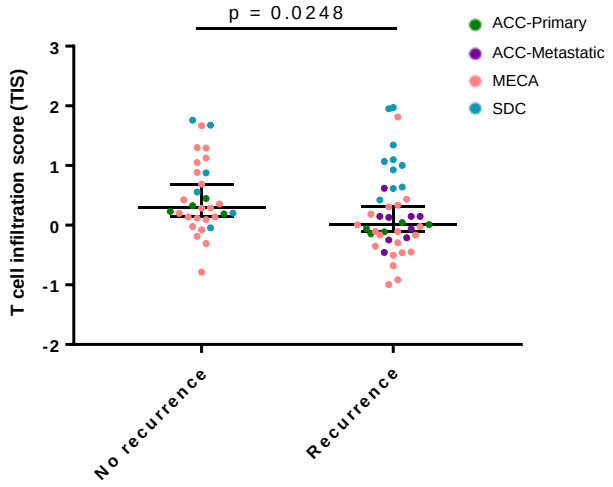

B

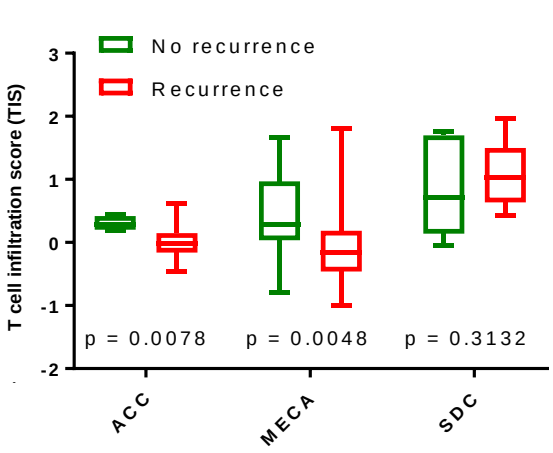

C

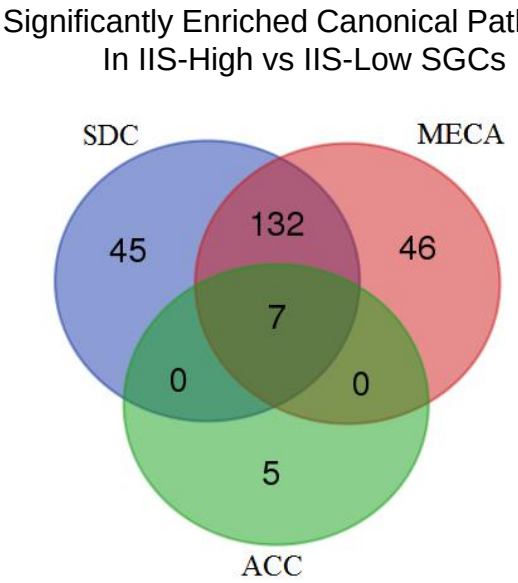

D

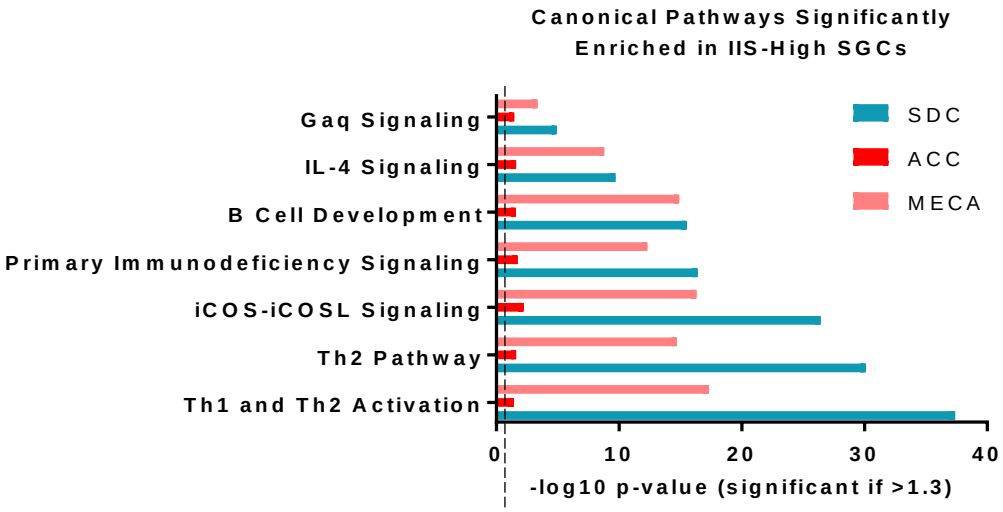

Author Manuscript Published OnlineFirst on February 14, 2020; DOI: 10.1158/1078-0432.CCR-19-3758
Author manuscripts have been peer reviewed and accepted for publication but have not yet been edited.

Figure 3

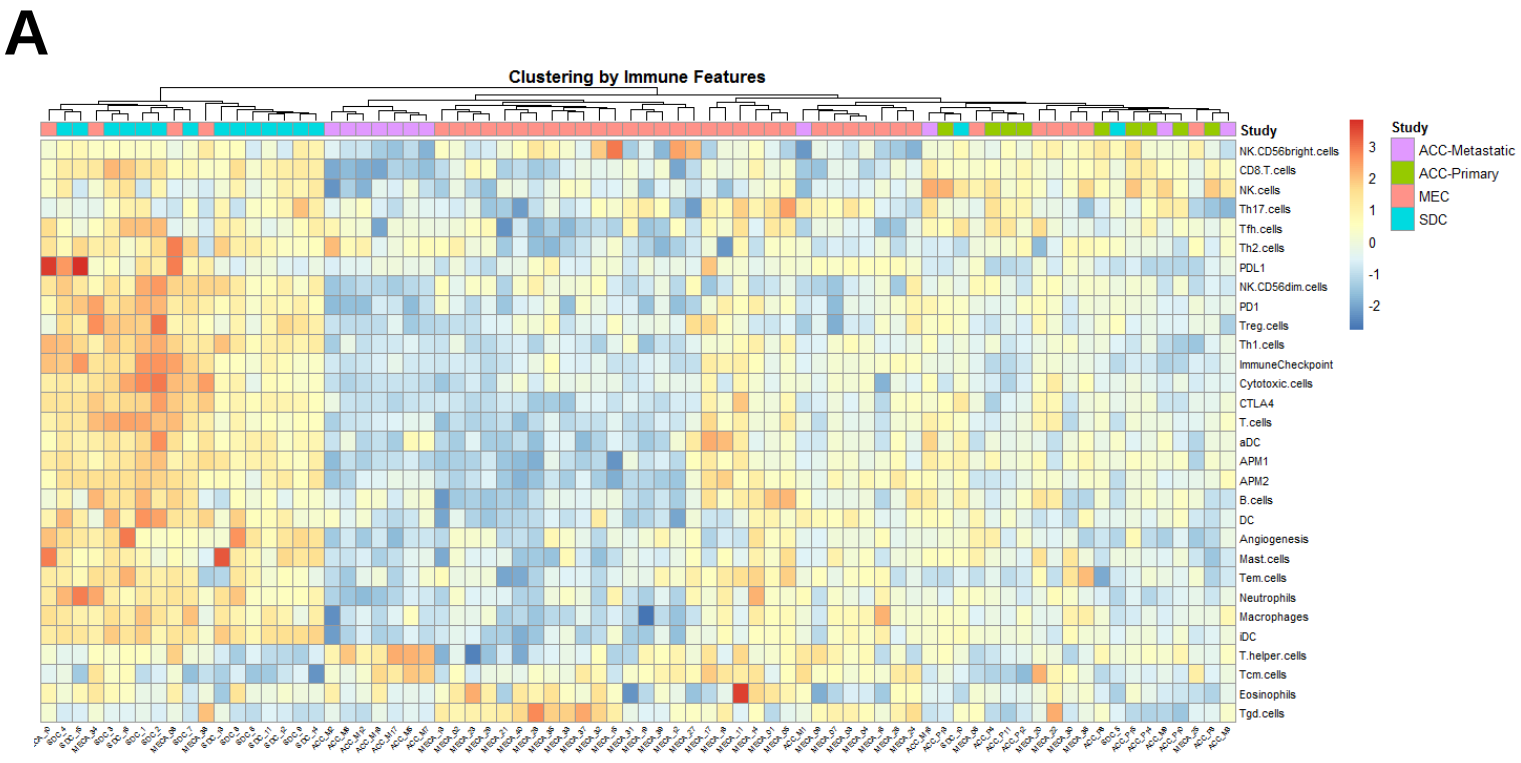

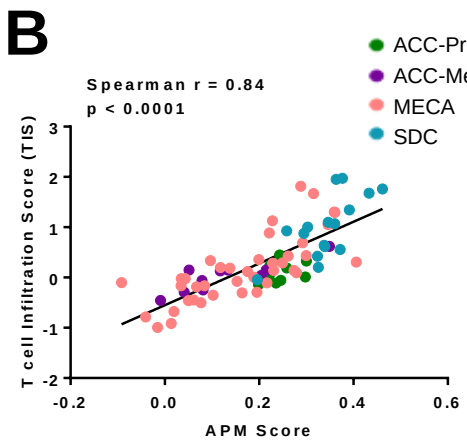

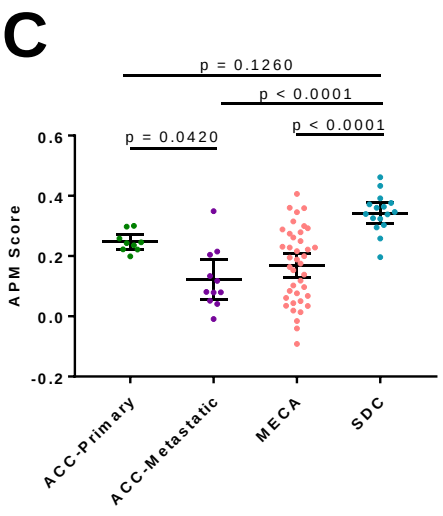

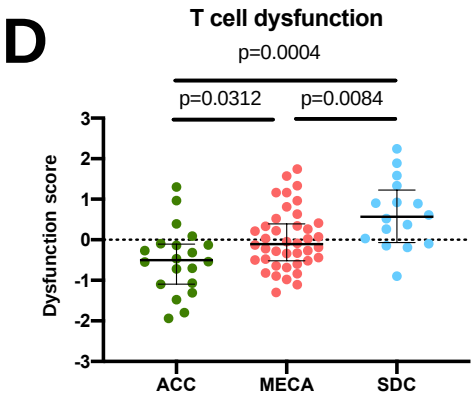

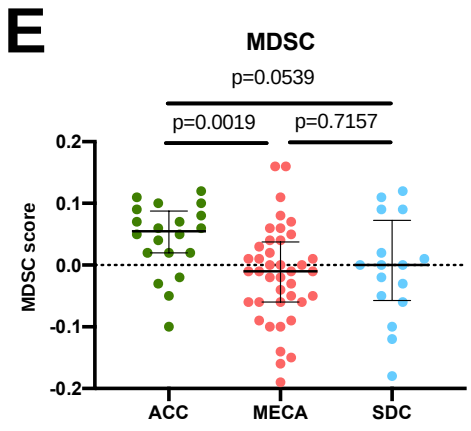

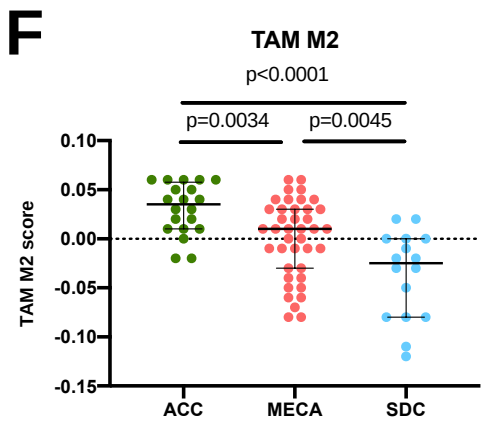

Author Manuscript Published OnlineFirst on February 14, 2020; DOI: 10.1158/1078-0432.CCR-19-3758
Author manuscripts have been peer reviewed and accepted for publication but have not yet been edited.

Figure 2

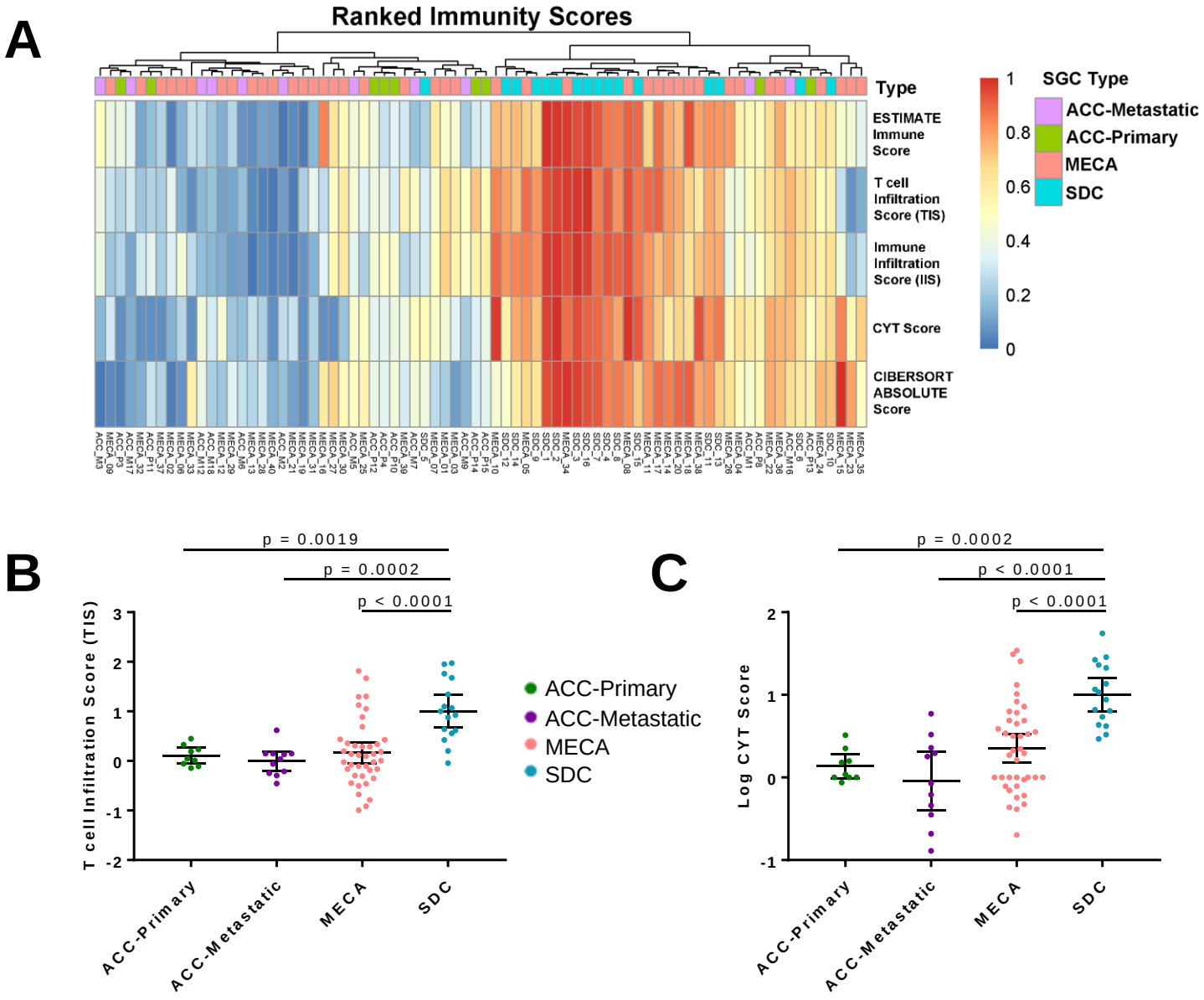

Author Manuscript Published OnlineFirst on February 14, 2020; DOI: 10.1158/1078-0432.CCR-19-3758
Author manuscripts have been peer reviewed and accepted for publication but have not yet been edited.

Figure 1

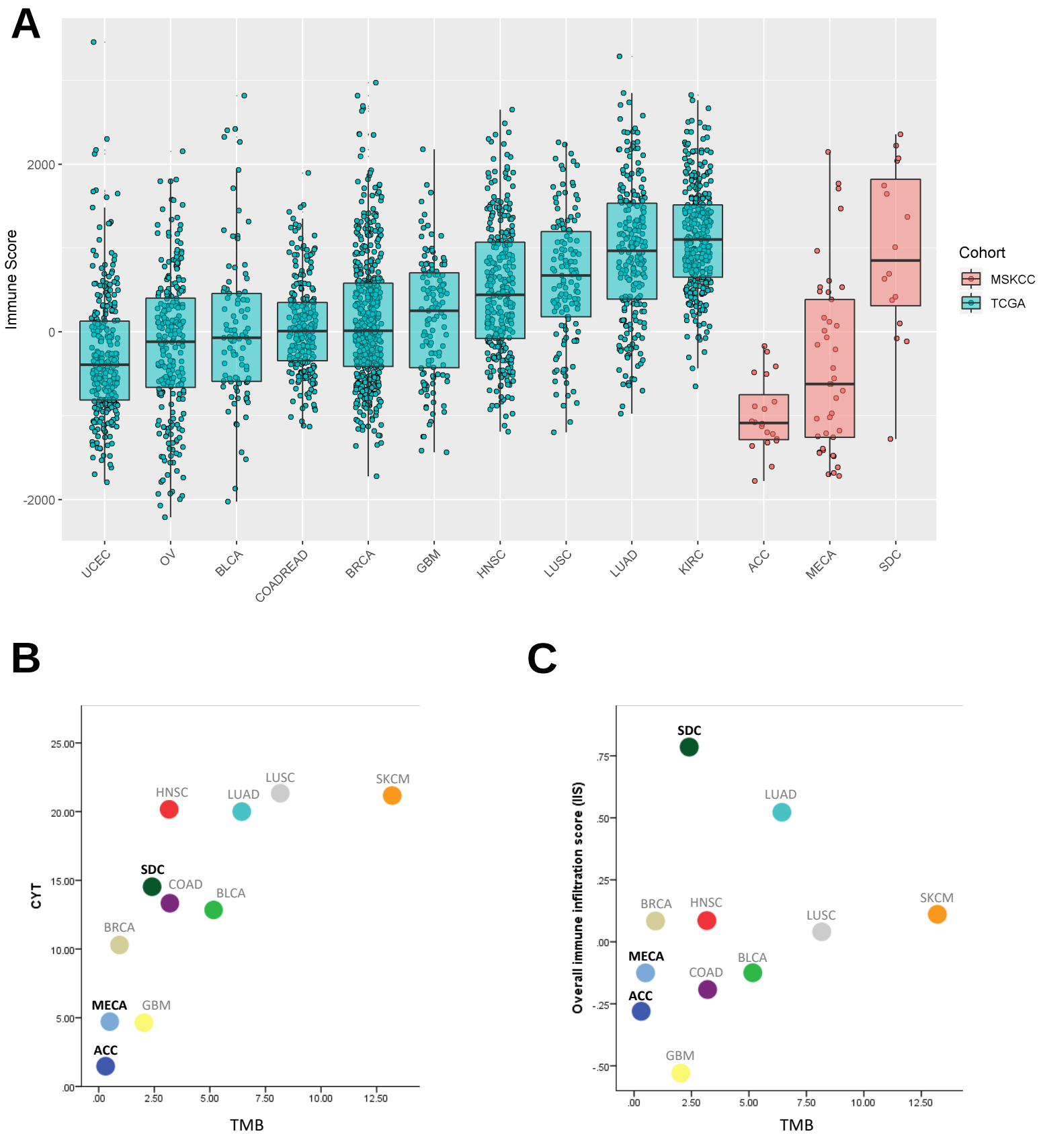

AACR American Association for Cancer Research

Clinical Cancer Research

The immune microenvironment and neoantigen landscape of aggressive salivary gland carcinomas differ by subtype

Luc GT Morris, Maximilian Linxweiler, Fengshen Kuo, et al.

Clin Cancer Res Published OnlineFirst February 14, 2020.